Gamma-protocadherin localization at the synapse corresponds to parameters of synaptic maturation

Nicole LaMassa[1,2], Hanna Sverdlov[2], Michael Bucaro[2], Monica Fernandez-Monreal[3], Greg R. Phillips[1,2,4]

[1]Program in Biology, Neuroscience Subprogram, CUNY Graduate Center
[2]Department of Biology, College of Staten Island, CUNY
[3]Bordeaux Imaging Center, French National Centre for Scientific Research
[4]Center for Developmental Neuroscience, College of Staten Island, CUNY

Address correspondence to:
Greg R. Phillips, PhD
Department of Biology
College of Staten Island, CUNY
2800 Victory Blvd.
Staten Island, NY 10314
Greg.Phillips@csi.cuny.edu

Running title: Role of synaptic gamma-protocadherins

Key words: Perforation, postsynaptic density, dendritic spine, immuno-electron microscopy

Acknowledgements: Supported by R03 MH110980 to GRP.

Abstract

Clustered protocadherins (Pcdhs) are a large family of ~60 cadherin-like proteins (divided into the subclasses α, β, and γ) that compose a surface "barcode" in individual neurons. The code is generated through combinatorial expression via epigenetic regulation at a large gene cluster that encodes the molecules. During early neural development, Pcdhs were shown to mediate dendrite self-recognition and avoidance in some neuronal types through a still uncharacterized anti-adhesive mechanism. Pcdhs have also been postulated to participate in synaptogenesis and the specificity of connectivity. Some synaptic defects were noted in knockout animals including synaptic number and physiology but the role of these molecules in synaptic development is not understood. We have shown previously that Pcdh-γs are highly enriched in intracellular compartments located in dendrites and spines with less frequent localization at the synaptic membrane. We compared synapses that expressed endogenous Pcdh-γs versus those that did not for parameters of synaptic maturation including pre- and postsynaptic punctum size, postsynaptic perforations and spine morphology in mature cultured hippocampal neurons. We also performed serial section immuno-electron microscopy in intact hippocampal CA1 and measured synaptic size and perforation status of Pcdh-γ positive and negative synapses. At both the light and ultrastructural levels, synapses immunopositive for Pcdh-γs were found to be larger in diameter with more frequent perforations. Analysis of spines in cultured neurons revealed that mushroom spines were more frequently immunopositive for Pcdh-γs at their tips than thin spines. Taken together, these results suggest that Pcdh-γ function at the synapse may be related to synaptic maturation and stabilization.

Introduction

The specificity of wiring of the vertebrate nervous system is achieved at several levels or stages during embryonic and postnatal development. Postmitotic neurons must elaborate dendritic arbors in the correct spatial orientation as well as send axons out along proper trajectories. Later in development, axons interact with the dendrite to form excitatory synapses. In large part, these developmental processes are facilitated by the action of cell-surface adhesion and recognition proteins (Kim, 2019) that allow neuronal outgrowths to sense their environment and respond accordingly.

It has been proposed that cell adhesion molecules also establish a system of suitable specificity that can restrict interactions between the enormous number of neurons and glial cells. One group of cell adhesion molecules, the clustered protocadherins (Pcdhs), a family of ~60 adhesion molecules encoded on a large gene cluster (Wu and Maniatis, 1999; Zipursky and Sanes, 2010), fulfills these criteria. Members of the three subclasses of Pcdhs (α, β, and γ) are expressed stochastically through epigenetic regulation (Guo et al., 2012; Hirayama et al., 2012; Monahan et al., 2012; Jiang et al., 2017). A combination of molecules from the three subclasses generates a unique homophilic recognition unit (Schreiner and Weiner, 2010; Goodman et al., 2016, 2017; Brasch et al., 2019) on neuronal surfaces.

In vertebrates, these cell-specific recognition units, presumed to be identical on the surfaces of same-cell dendrites, most likely are primary mediators of dendritic self-avoidance in certain neurons that have planar dendrites such as the retinal starburst amacrine cell and the cerebellar Purkinjie cell, as demonstrated in Pcdh-γ conditional null animals (Lefebvre et al., 2012; Ing-Esteves et al., 2018). Other roles for Pcdhs in dendrite elaboration have been observed that do not involve same-cell recognition but rather astrocyte-dendrite interaction (Garrett and Weiner, 2009; Molumby et al., 2016) in cortical neurons. It is possible that there are different modes of Pcdh interactions, those between same cell processes and those between

different cells and that these modes may have different outcomes in terms of positive or negative effects on cell adhesion.

Overall, the roles of Pcdhs in early neurodevelopmental events, such as dendrite (Garrett and Weiner, 2009; Molumby et al., 2016) and axon (Hasegawa et al., 2008, 2012, 2016; Prasad and Weiner, 2011; Chen et al., 2017; Katori et al., 2017; Lu et al., 2018) outgrowth, have been the most studied. However, Pcdhs remain expressed long after these events have completed (Phillips et al., 2003; Frank et al., 2005). Pcdhs are located at some excitatory synapses at 1 month postnatally in rodents at the synaptic cleft and within intracellular synaptic compartments in vivo and in cultures (Wang et al., 2002; Phillips et al., 2003; Fernández-Monreal et al., 2009, 2010). Pcdhs have been shown to participate in synaptic development but the exact role may depend on cell type. For example, mice lacking Pcdh-γs exhibit deficits in synaptic numbers and physiology in spinal cord neurons (Weiner et al., 2005) and increased synapses in cortical neurons (Molumby et al., 2017). Pcdh-γs can interact with various synaptic and signaling molecules (Chen et al., 2009; Han et al., 2010; Garrett et al., 2012; Keeler et al., 2015; Mah et al., 2016; Molumby et al., 2017; Fan et al., 2018) but which of these coordinate with Pcdhs to affect synaptic development is still unknown. It has been hypothesized that Pcdhs play a role in late synaptic developmental events (Jontes and Phillips, 2006).

It is known that synaptic stability and maturation are associated with a widening of the synapse and dendritic spine head (reviewed in (Berry and Nedivi, 2017)). The appearance of perforations in the postsynaptic density has also been associated with an increased number of AMPA receptors which is suggestive of a mature and strengthened synapse (Desmond and Weinberg, 1998; Lüscher et al., 2000; Nicholson et al., 2006).

Antibodies that detect Pcdh-γs label striking punctate structures in vivo and in cultured hippocampal neurons that are thought to represent trafficking organelles but also, at times,

overlapped with synaptic markers (Wang et al., 2002; Phillips et al., 2003; Fernández-Monreal et al., 2009, 2010). We asked whether synapses positive for Pcdh-γs exhibit differences in terms of diameter and perforation status relative to unlabeled synapses. Using serial section immuno-electron microscopy in vivo and confocal microscopy of immunolabeled cultured neurons we compared synapses that harbor Pcdh-γs to those that do not for these parameters of synaptic maturation. We found that Pcdh- γ positive synapses were significantly larger and were more likely to be perforated. When Pcdh-γs were located near the tip of the dendritic spine, that spine was more likely to be of the mushroom type. These results suggest that Pcdh-γs could be associated with stabilization and maturation events of excitatory synapses in hippocampus.

Materials and Methods

Hippocampal neuron cultures and labeling

Neurons were cultured from embryonic day 18 rat embryos as described previously (Phillips et al., 2003; Fernández-Monreal et al., 2009) and grown for 22 days. In some cases, neurons were transfected at day 15 with pEGFP-n1 to fill dendrites with GFP and grown for an additional 7 days as described (Fernández-Monreal et al., 2009). For synaptic measurements, neurons were fixed and immunolabeled with an affinity purified antibody raised against the Pcdh-γ constant cytoplasmic domain (Phillips et al., 2003) and colabeled with goat anti-PSD-95 (Abcam Cat# ab12093, RRID:AB_298846) and mouse anti-vGlut (Millipore Cat# MAB5502, RRID:AB_262185). For spine measurements, GFP filled neurons were stained with anti-Pcdh-γ only.

Confocal image analysis

Images were obtained with a Zeiss LSM510 META confocal microscope. Double and triple label z-stack images were acquired in multi-track mode at 4 times line averaging with a 63x/1.4 NA oil DIC objective. Z-stacks were flattened by maximum projection for image analysis. Images were imported into NIH Image J as separate channels for colocalization analysis. The

Pcdh-γ channel was merged separately with the PSD-95 channel or the vGlut channel. Pixels in which Pcdh-γ colocalized with either synaptic marker were detected with the RG2B colocalization plugin which generates a new image of the colocalized pixels. The colocalization images were used to map and save regions of interest (ROIs) using the ROI manager in Image J. Synapses that did not show Pcdh-γ colocalization with PSD-95 and/or vGlut were also mapped. To identify synapses in which Pcdh-γs overlapped simultaneously with PSD-95 and vGlut, images representing the colocalized pixels from Pcdh-γ/PSD-95 and Pcdh-γ/vGlut were loaded into separate channels and subjected again to the RG2B colocalization plugin which resulted in an image map containing pixels of colocalization for all three markers. ROIs of synapses from Pcdh-γ/PSD-95, Pcdh-γ/vGlut and Pcdh-γ/PSD-95/vGlut colocalization, as well as unlabeled synapses, were saved and remapped onto the original single channel PSD-95 or vGlut images. The area and average pixel value of the synaptic PSD-95 and vGlut punctum was determined in Image J for all synapses and averaged over 3 neurons. In addition, the number of PSD-95 puncta associated with each vGlut punctum was noted and synapses were categorized as macular for 1 PSD-95 punctum associated with the vGlut punctum or “split” for two distinct PSD-95 puncta associated with a single vGlut punctum. The percentage for macular versus split PSD synapses were averaged for the total population and compared to Pcdh-γ positive synapses in 3 neurons.

Animals

All animals used in this study were in accordance with the Institutional Care and Use Committee (IACUC). Postnatal day 30 Sprague-Dawley rats were prepared for electron microscopy by freeze substitution and low temperature embedding as described previously (Fernández-Monreal et al., 2010).

Serial sectioning

The block was roughly trimmed using a single edge, heavy duty razor blade. Then, it was finely trimmed to include a narrow area of CA1 including the pyramidal layer and stratum radiatum using a Diatome trimtool 20 (Diatome). Serial 70 nm sections were cut with a 45° diamond knife (Diatome) using a Leica UCT Ultramicrotome. Ribbons of ~5 sections were oriented and collected on formvar/carbon coated nickel slot grids (Electron Microscopy Sciences) using a perfect loop (Electron Microscopy Sciences).

Postembed immunogold labeling and staining

Grids were loaded into a Chien staining pad (Ted Pella) and sections were immunolabeled with an affinity-purified rabbit polyclonal antibody generated against the mouse Pcdh-γ constant cytoplasmic domain (Phillips et al., 2003) diluted 1:5 in 20 mM Tris pH 7.4, 20 mM NaCl, 3% BSA and 1% Triton-X 100 overnight in a humidified chamber. The sections were then washed three times with 20 mM Tris pH 7.4, 20 mM NaCl and incubated with secondary 15 nm gold-tagged goat-anti-rabbit IgG F(ab')2 (Electron Microscopy Sciences) diluted 1:10 in 20 mM Tris pH 7.4, 20 mM NaCl, 3% BSA and 1% Triton-X 100, overnight in a humidified chamber. The grids were washed again three times and then rinsed once with deionized water.

The sections were stained with 4% uranyl acetate for 40 minutes in a dark chamber and washed three times with deionized water. The grids were then stained with Reynold's lead citrate for 30 seconds and washed three times with deionized water. The grids were left to dry before imaging.

Acquisition of serial images and EM image analysis

Serial images of CA1 stratum radiatum were acquired using a Fei Tecnai Spirit Transmission Electron Microscope (Advanced Imaging Facility, College of Staten Island) at 18,500x magnification. Identification of corresponding areas of stratum radiatum in each consecutive section was facilitated using blood vessels as landmarks.

Image series were saved as stacks in Image J. Every synapse in each stack was identified, the diameter of the postsynaptic density was measured using the section through the

widest part of the synapse in the serial images. Synapse status as macular or perforated was compiled visually from the serial images. A synapse was considered labeled if it contained at least two gold particles on its cleft, spine or axonal compartment in a section. The average diameter of labeled or unlabeled synapses was compared and statistical significance determined by t test.

Results

Pcdh-γ localization at synapses is associated with larger synaptic puncta and "split" PSD puncta

Previous studies have shown Pcdh-γs to be localized at a subset of synapses in vivo (Wang et al., 2002) and in cultured neurons (Phillips et al., 2003) but the role of these molecules in synaptic development remains unknown. Some defects in synaptic number and physiology in in Pcdh-γ null animals have been noted (Weiner et al., 2005; Molumby et al., 2017) suggesting the possibility that Pcdh-γs might participate in synaptic maturation or stability. Synapse size is one parameter that can be associated with synaptic stability (Berry and Nedivi, 2017). We identified Pcdh-γ positive synapses in 21 day old cultured hippocampal neurons (Fig. 1A) using an unbiased selection based on overlap of signal from Pcdh-γ immunolabeling with the signal for both pre and postsynaptic makers (Fig. 1B). Using this selection, 19% of synapses were considered Pcdh-γ positive (a Pcdh-γ punctum overlapping with both pre- and postsynaptic markers simultaneously), 17% synapses lacked any Pcdh-γ labeling overlapping with either pre- or postsynaptic markers, and 64% exhibited a Pcdh-γ punctum overlapping with a pre- and/or postsynaptic specialization but not simultaneously (n=301 synapses from 3 neurons).

We compared the area of pre- and postsynaptic puncta for three categories of synapses: Those positive for Pcdh-γ immunoreactivity simultaneously overlapping with both pre- and postsynaptic markers (correlated label) (Fig. 2A), those with Pcdh-γ immunoreactivity overlapping with either pre- or postsynaptic puncta but not simultaneously (uncorrelated label) (Fig. 2B) and synapses with no overlapping Pcdh-γ immunoreactivity (unlabeled) (Fig. 2C). It

was found that synapses with uncorrelated label exhibited similar pre- and postsynaptic areas to those of unlabeled synapses, while, in contrast, synapses with correlated label exhibited a larger presynaptic and postsynaptic puncta area (Fig. 2D). In contrast, no differences were observed in average pixel value of the pre- or postsynaptic label for all types of synapses.

During the course of measuring synaptic puncta area, it was noted that many Pcdh-γ positive synapses (correlated label) exhibited discontinuous PSD puncta in contact with a single presynaptic punctum suggestive of synaptic perforation. Overall, these split PSD synapses amounted to about 34% of the total population. However, of the Pcdh-γ positive synapses with simultaneous pre- and postsynaptic label, a significantly larger percentage (59%) were split PSD synapses (Fig. 3). These results indicate Pcdh-γs correspond to a distinct class of synapses with morphological characteristics, at the light level, that resemble perforated synapses.

Serial immuno-EM analysis of anti-Pcdh-γ labeled synapses in vivo

The light level observations suggested that synaptic Pcdh-γs delinate maturing synapses with larger synaptic specializations and with the possibility of increased perforated PSDs. To study this in more detail in vivo, Pcdh-γ antibodies were used to label serial sections of rat hippocampal CA1 at 30 days postnatal, which is a period of ongoing synaptic development (Harris et al., 1992). Using serial sectioning, labeled synapses can be identified and synaptic parameters, such as the diameter of the synapse, as well as perforation status, accurately quantified taking adjacent sections into account. In many instances, gold particles labeled the same structure in multiple sections (arrows and double arrowheads, Fig. 4). Overall, Pcdh-γ labeling was found at some synaptic clefts (double arrowheads, Fig. 4), synaptic (double arrows, Fig. 4) and non-synaptic (arrowheads, Fig. 4) intracellular compartments and at non-synaptic cell-cell contact points (asterisk, Fig. 4), as previously reported.

Quantitative comparison of anti-Pcdh-γ-labeled and unlabeled synapses was performed. The diameter of every synapse was measured through the widest part of each synapse in serial sections (n=140 synapses in 21 serial image stacks). Each synapse was also classified as either macular or perforated. Synapses were then categorized as anti-Pcdh-γ labeled or unlabeled. The majority of Pcdh-γ labeled synapses were immunopositive for Pcdh-γ within intracellular compartments as previously described (Fernández-Monreal et al., 2010). Therefore synapses were considered as labeled if multiple gold particles were present over the same subcellular structure either at the cleft or within an dendritic or axon compartment, or some combination thereof. Overall, it was found that Pcdh- γ labeled synapses exhibited an average diameter of 484 nm which was significantly larger when compared to unlabeled synapses, that averaged 222 nm in diameter (Fig. 5A).

To determine if Pcdh-γ positive synapses are more likely to be perforated, synapses were classified as macular or perforated through examination of serial sections (Fig. 5A). Of the 78 unlabeled synapses, only 2 were perforated, while in contrast, among the 106 labeled synapses, 16 were perforated, which was a signficant difference (Fig. 5C).

Pcdh-γ position in dendritic spine heads corresponds to a mushroom type

The Pcdh-γ immunostaining pattern at the light level is strikingly discrete, with puncta that can localize at the spine head, neck or dendritic shaft (Fernández-Monreal et al., 2009). Mushroom type spines are thought to be the most stable spines while thin spines are more transient (reviewed in (Berry and Nedivi, 2017). To examine the relationship between Pcdh-γ expression at the spine and spine morphology, we transfected primary neurons with GFP which were then grown for 21 days, fixed and immunostained with anti-Pcdh-γ (Fig. 6A). All spines were first categorized as being either mushroom, thin or stubby then the location of Pcdh-γ puncta was assigned to either the spine head (‘a’, Fig. 6B), the spine neck (‘b’, Fig. 6B) or the

dendritic shaft at the spine base ('c', Fig. 6B). There were relatively few stubby spines in these neurons and these spines were therefore excluded from further analysis.

Many spines were unlabeled, consistent with the variability of Pcdh-γ localization at synapses reported previously (Wang et al., 2002; Phillips et al., 2003). When present at spines, the most frequent location for Pcdh-γ puncta in both mushroom and thin spines was in the spine head. However, many spines were also labeled at the spine neck with a smaller number labeled at the base of the spine in the dendritic shaft.

Most (51%) of the mushroom spines were labeled at the spine head which differed with thin spines that were less frequently labeled at the spine head (Fig. 6D, upper left). In contrast, Pcdh-γ labeling at spine necks or the base was not predictive of spine type; neither were unlabeled spines predominately of any one type (Fig. 6D). These results suggest that Pcdh-γs could be associated with some aspect of spine maturation.

Discussion

The Pcdh gene cluster is capable of generating, through epigenetic regulation of ~60 different isoforms (Guo et al., 2012; Hirayama et al., 2012; Monahan et al., 2012; Yin et al., 2017), what has been considered an adhesive "barcode" (Rubinstein et al., 2017; Mountoufaris et al., 2018) on the surfaces of individual neurons. What this code does during neural development is still being elaborated. In vivo, one of the most well-characterized functions for Pcdhs is in repulsion, both in the self-avoidance of same-cell dendrites and in repulsion or organization of certain axon tracts (Hasegawa et al., 2008, 2012, 2016; Katori et al., 2009, 2017; Prasad and Weiner, 2011; Chen et al., 2017; Lu et al., 2018). These are developmental processes that occur throughout embryonic and early postnatal development. However, Pcdhs are also highly expressed at later stages of development where synaptogenesis is prominent (Frank et al., 2005). The role of these molecules in synaptogenesis is currently unknown but some synaptic defects have been observed in Pcdh-γ null animals. Here we find that synapses

with Pcdh-γ expression are significantly larger and have more perforations suggesting that these synapses may be more mature and/or stable.

Prior to synaptogenesis, dendrites elaborate an arbor that must occupy a distinct territory in the neuropil. In some neurons with planar dendritic trees, such as starbust amacrine cells in the retina or cerebellar Purkinje cells, same-cell dendrites rarely cross but can overlap with dendrites from neighboring neurons. It was shown in Pcdh-γ deficient mice that the dendrites from these neurons exhibited defective spatial distribution and abnormal clumping of the dendrites (Lefebvre et al., 2012; Ing-Esteves et al., 2018). In early stage hippocampal cultures, which are also planar, Pcdh-γs align precisely at what have been termed “dendritic bridges” that could be morphological correlates of self-avoidance (Fernández-Monreal et al., 2009; Phillips et al., 2017). For avoidance to happen, it is almost certain that Pcdhs first make an adhesive linkage at contacting same-cell dendrites followed by detachment, cleavage or endocytosis of the adhesive complex in order for the contacting membranes to separate and dendrites to adopt different trajectories. These same cell contacts are most likely to have a perfectly matching repertoire of Pcdhs. In contrast, Pcdh adhesive complexes at heterotypic junctions such as synapses or perisynaptic astrocyte contacts might have an “imperfect” match of Pcdhs that may behave differently than at same-cell contacts. Thus, our results, combined with others, suggest the possibility that Pcdhs may play different roles depending on context, with an avoidance role for dendrites of certain neurons and adhesive role in other instances.

During synaptic development, synapses make an initial adhesive contact through an expanding array of adhesion molecules (Kim, 2019). During postnatal life, robust synaptogenesis occurs but many presumptively functional synapses are also pruned. One possibility, based on their role in repulsion of same-cell dendrites, is that Pcdh adhesion participates in the synaptic pruning process. It would then be likely that synapses that exhibit Pcdh expression might exhibit a less mature phenotype than those that lack Pcdhs. The other

possibility suggested by the present study is that Pcdh adhesion strengthens and stabilizes synaptic connections. It has been shown in vivo that the most persistent and stable spines have the widest diameter and a mushroom shape while transient spines are narrower (Berry and Nedivi, 2017). In the present study, synapses labeled with anti-Pcdh-γ were significantly wider and more likely to be perforated, both in vivo and in culture, and spine morphology was more likely to be of the mushroom type in culture.

How might the endocytic trafficking model fit into the stabilization of synapses/spines?

Synapse stabilization is more consistent with an adhesive-like, rather than repulsive, role between pre- and postsynaptic neurons. Many of the synapses labeled in the present study were labeled intracellularly in addition to at the cleft. A model for Pcdh-mediated cell repulsion has been proposed in which an adhesive match between Pcdhs on adjacent cells induces rapid endocytosis which could remove other adhesive complexes from the cell surface and cause cell detachment (Phillips et al., 2017). How such a mechanism could be associated with synapse stabilization is not clear. Our results show that Pcdh-γs are associated with more mature synapses but whether this involves a structural adhesive function is currently unknown. It is possible that endocytosis of Pcdhs after adhesive contact triggers a signaling mechanism that contributes to synapse stabilization. Overall our results do indicate that Pcdh-γs are likely to be part of a synaptic maturation process with timely implications given the emerging role of Pcdh misregulation in neurodevelopmental disorders (El Hajj et al., 2017).

Figure legends

Figure 1. Unbiased selection of Pcdh-γ positive synapses in hippocampal neurons triple-labeled with antibodies to vesicular glutamate transporter (vGlut; blue channel), PSD-95 (red channel), and anti-Pcdh-γ constant domain (green channel). (A) Low magnification image of a single labeled neuron. Note the concentration of Pcdh-γ labeled puncta in the cell

body and interior portion of dendrites consistent with a largely intracellular localization for Pcdh-γs in an intracellular compartment as reported previously. (B-F) Higher magnification of a dendrite and selection of pixels corresponding to Pcdh-γ label that overlaps with vGlut, PSD-95, or both simultaneously. (B) vGlut/PSD-95 labeling pattern showing synapses along dendrite. (C) Overlay of image in (B) with Pcdh-γ signal. (D) Image generated from pixels in which Pcdh-γ signal overlaps with that of PSD-95. (E) Image generated from pixels in which Pcdh-γ signal overlaps with that of vGlut. (F) The image data in (D) and (E) loaded into the red and green channels of a new image and overlapping pixels selected. These map to synapses in which Pcdh-γ label overlaps with both vGlut and PSD-95 simultaneously (arrowheads in B-F). Bar = 10 μm.

Figure 2. Area and average pixel value of pre- and postsynaptic profiles for Pcdh-γ negative synapses or synapses in which Pcdh-γ label overlaps with one or both synaptic markers simultaneously. (A) Examples of synapses in which Pcdh-γ signal overlaps with either vGlut or PSD-95 but not simultaneously. (B) Example of a synapse in which the Pcdh-γ signal overlaps with both vGlut and PSD-95 simultaneously. (C) Example of a Pcdh-γ negative synapse. (D) Quantification of area and average pixel values for pre- (left) and postsynaptic (right) puncta for the three categories of synapses. When Pcdh-γ correlates with both pre- and postsynaptic puncta simultaneously there was a significant increase in the area of both puncta ($p<0.05$).

Figure 3. Pcdh-γ positive synapses are more likely to exhibit segmented PSD-95 puncta associated with a single presynaptic profile. (A and B) Example of a confocal z-stack of a single synapse in which Pcdh-γ signal overlaps with vGlut and PSD-95 simultaneously. Top panels show triple labeling while bottom panels show only vGlut and PSD-95. Arrows point to

distinct PSD-95 puncta associated with a single vGlut punctum (arrowhead). (C) Quantification of percentage of split PSD-95 synapses. Of the Pcdh-γ positive synapses, ~60% were split PSD-95 synapses while the total population on exhibited ~38% split PSD-95 profiles ($p<0.001$). Bar = 1 μm.

Figure 4. Immuno-EM serial section analysis of synapses labeled with anti-Pcdh-γ. Five serial sections through a synapse positive for Pcdh-γs at the cleft (double arrowheads) and an internal dendritic compartment (double arrows). Bar = 500 nm.

Figure 5. Pcdh-γ synapses have larger diameter and are more likely to be perforated. (A) Serial sections through Pcdh-γ positive synapses. Pcdh-γ labeling at clefts and synaptic compartments indicated by an arrowhead. Some Pcdh-γ positive synapses were macular (top) while others were revealed to be perforated (brackets, bottom) upon serial sectioning. Bar = 500 nm. (B) Quantification of synapse diameter for Pcdh-γ labeled versus unlabeled synapses. Unlabeled synapses averaged 200 nm in diameter while labeled synapses were more than twice as large at 400 nm in diameter ($p<0.005$). (C) The overwhelming majority of unlabeled synapses were macular type synapses while ~20% of labeled synapses were perforated (chi-squared test=0.01).

Figure 6. Mushroom spine heads are more likely to be Pcdh-γ positive than thin spine heads. (A) GFP (green channel) filled neuron labeled with anti-Pcdh-γ (red channel). (B) Categorization of labelling patterns based on location of Pcdh-γ positive puncta with the spine ('a' denotes spine head labeling, 'b', spine neck labeling and 'c', shaft labeling directly below the spine). (C) Distribution of spine type with respect to labeling pattern. (D) Quantification of the proportion of thin or mushroom spines that exhibit the indicated labeling pattern. The proportion

of unlabeled, spine neck labeled, or dendritic shaft labeled spines was not significantly different between thin and mushroom spines while spines that were labeled on the head were more likely to be mushroom type spines ($p<0.05$) Bar= 10 μm.

References

Berry KP, Nedivi E. 2017. Spine Dynamics: Are They All the Same? Neuron 96:43–55.

Brasch J, Goodman KM, Noble AJ, Rapp M, Mannepalli S, Bahna F, Dandey VP, Bepler T, Berger B, Maniatis T, Potter CS, Carragher B, Honig B, Shapiro L. 2019. Visualization of clustered protocadherin neuronal self-recognition complexes. Nature.

Chen J, Lu Y, Meng S, Han M-H, Lin C, Wang X. 2009. alpha- and gamma-Protocadherins negatively regulate PYK2. J Biol Chem 284:2880–2890.

Chen WV, Nwakeze CL, Denny CA, O'Keeffe S, Rieger MA, Mountoufaris G, Kirner A, Dougherty JD, Hen R, Wu Q, Maniatis T. 2017. Pcdhαc2 is required for axonal tiling and assembly of serotonergic circuitries in mice. Science 356:406–411.

Desmond NL, Weinberg RJ. 1998. Enhanced expression of AMPA receptor protein at perforated axospinous synapses. Neuroreport 9:857–860.

El Hajj N, Dittrich M, Haaf T. 2017. Epigenetic dysregulation of protocadherins in human disease. Semin Cell Dev Biol 69:172–182.

Fan L, Lu Y, Shen X, Shao H, Suo L, Wu Q. 2018. Alpha protocadherins and Pyk2 kinase regulate cortical neuron migration and cytoskeletal dynamics via Rac1 GTPase and WAVE complex in mice. Elife 7.

Fernández-Monreal M, Kang S, Phillips GR. 2009. Gamma-protocadherin homophilic interaction and intracellular trafficking is controlled by the cytoplasmic domain in neurons. Mol Cell Neurosci 40:344–353.

Fernández-Monreal M, Oung T, Hanson HH, O'Leary R, Janssen WG, Dolios G, Wang R, Phillips GR. 2010. γ-protocadherins are enriched and transported in specialized vesicles associated with the secretory pathway in neurons. Eur J Neurosci 32:921–931.

Frank M, Ebert M, Shan W, Phillips GR, Arndt K, Colman DR, Kemler R. 2005. Differential expression of individual gamma-protocadherins during mouse brain development. Mol Cell Neurosci 29:603–616.

Garrett AM, Schreiner D, Lobas MA, Weiner JA. 2012. γ-protocadherins control cortical dendrite arborization by regulating the activity of a FAK/PKC/MARCKS signaling pathway. Neuron 74:269–276.

Garrett AM, Weiner JA. 2009. Control of CNS synapse development by {gamma}-protocadherin-mediated astrocyte-neuron contact. J Neurosci 29:11723–11731.

Goodman KM, Rubinstein R, Dan H, Bahna F, Mannepalli S, Ahlsén G, Aye Thu C, Sampogna RV, Maniatis T, Honig B, Shapiro L. 2017. Protocadherin cis-dimer architecture and recognition unit diversity. Proc Natl Acad Sci USA 114:E9829–E9837.

Goodman KM, Rubinstein R, Thu CA, Bahna F, Mannepalli S, Ahlsén G, Rittenhouse C, Maniatis T, Honig B, Shapiro L. 2016. Structural Basis of Diverse Homophilic Recognition by Clustered α- and β-Protocadherins. Neuron 90:709–723.

Guo Y, Monahan K, Wu H, Gertz J, Varley KE, Li W, Myers RM, Maniatis T, Wu Q. 2012. CTCF/cohesin-mediated DNA looping is required for protocadherin α promoter choice. Proc Natl Acad Sci USA 109:21081–21086.

Han M-H, Lin C, Meng S, Wang X. 2010. Proteomics analysis reveals overlapping functions of clustered protocadherins. Mol Cell Proteomics 9:71–83.

Harris KM, Jensen FE, Tsao B. 1992. Three-dimensional structure of dendritic spines and synapses in rat hippocampus (CA1) at postnatal day 15 and adult ages: implications for the maturation of synaptic physiology and long-term potentiation. J Neurosci 12:2685–2705.

Hasegawa S, Hamada S, Kumode Y, Esumi S, Katori S, Fukuda E, Uchiyama Y, Hirabayashi T, Mombaerts P, Yagi T. 2008. The protocadherin-alpha family is involved in axonal coalescence of olfactory sensory neurons into glomeruli of the olfactory bulb in mouse. Mol Cell Neurosci 38:66–79.

Hasegawa S, Hirabayashi T, Kondo T, Inoue K, Esumi S, Okayama A, Hamada S, Yagi T. 2012. Constitutively expressed Protocadherin-α regulates the coalescence and elimination of homotypic olfactory axons through its cytoplasmic region. Front Mol Neurosci 5:97.

Hasegawa S, Kumagai M, Hagihara M, Nishimaru H, Hirano K, Kaneko R, Okayama A, Hirayama T, Sanbo M, Hirabayashi M, Watanabe M, Hirabayashi T, Yagi T. 2016. Distinct and Cooperative Functions for the Protocadherin-α, -β and -γ Clusters in Neuronal Survival and Axon Targeting. Front Mol Neurosci 9:155.

Hirayama T, Tarusawa E, Yoshimura Y, Galjart N, Yagi T. 2012. CTCF is required for neural development and stochastic expression of clustered Pcdh genes in neurons. Cell Rep 2:345–357.

Ing-Esteves S, Kostadinov D, Marocha J, Sing AD, Joseph KS, Laboulaye MA, Sanes JR, Lefebvre JL. 2018. Combinatorial Effects of Alpha- and Gamma-Protocadherins on Neuronal Survival and Dendritic Self-Avoidance. J Neurosci 38:2713–2729.

Jiang Y, Loh Y-HE, Rajarajan P, Hirayama T, Liao W, Kassim BS, Javidfar B, Hartley BJ, Kleofas L, Park RB, Labonte B, Ho S-M, Chandrasekaran S, Do C, Ramirez BR, Peter CJ, C W JT, Safaie BM, Morishita H, Roussos P, Nestler EJ, Schaefer A, Tycko B, Brennand KJ, Yagi T, Shen L, Akbarian S. 2017. The methyltransferase SETDB1 regulates a large neuron-specific topological chromatin domain. Nat Genet 49:1239–1250.

Jontes JD, Phillips GR. 2006. Selective stabilization and synaptic specificity: a new cell-biological model. Trends Neurosci 29:186–191.

Katori S, Hamada S, Noguchi Y, Fukuda E, Yamamoto T, Yamamoto H, Hasegawa S, Yagi T. 2009. Protocadherin-alpha family is required for serotonergic projections to appropriately innervate target brain areas. J Neurosci 29:9137–9147.

Katori S, Noguchi-Katori Y, Okayama A, Kawamura Y, Luo W, Sakimura K, Hirabayashi T, Iwasato T, Yagi T. 2017. Protocadherin-αC2 is required for diffuse projections of serotonergic axons. Sci Rep 7:15908.

Keeler AB, Schreiner D, Weiner JA. 2015. Protein Kinase C Phosphorylation of a γ-Protocadherin C-terminal Lipid Binding Domain Regulates Focal Adhesion Kinase Inhibition and Dendrite Arborization. J Biol Chem 290:20674–20686.

Kim B. 2019. Evolutionarily conserved and divergent functions for cell adhesion molecules in neural circuit assembly. J Comp Neurol.

Lefebvre JL, Kostadinov D, Chen WV, Maniatis T, Sanes JR. 2012. Protocadherins mediate dendritic self-avoidance in the mammalian nervous system. Nature 488:517–521.

Lu W-C, Zhou Y-X, Qiao P, Zheng J, Wu Q, Shen Q. 2018. The protocadherin alpha cluster is required for axon extension and myelination in the developing central nervous system. Neural Regen Res 13:427–433.

Lüscher C, Nicoll RA, Malenka RC, Muller D. 2000. Synaptic plasticity and dynamic modulation of the postsynaptic membrane. Nat Neurosci 3:545–550.

Mah KM, Houston DW, Weiner JA. 2016. The γ-Protocadherin-C3 isoform inhibits canonical Wnt signalling by binding to and stabilizing Axin1 at the membrane. Sci Rep 6:31665.

Molumby MJ, Anderson RM, Newbold DJ, Koblesky NK, Garrett AM, Schreiner D, Radley JJ, Weiner JA. 2017. γ-Protocadherins Interact with Neuroligin-1 and Negatively Regulate Dendritic Spine Morphogenesis. Cell Rep 18:2702–2714.

Molumby MJ, Keeler AB, Weiner JA. 2016. Homophilic Protocadherin Cell-Cell Interactions Promote Dendrite Complexity. Cell Rep 15:1037–1050.

Monahan K, Rudnick ND, Kehayova PD, Pauli F, Newberry KM, Myers RM, Maniatis T. 2012. Role of CCCTC binding factor (CTCF) and cohesin in the generation of single-cell diversity of protocadherin-α gene expression. Proc Natl Acad Sci USA 109:9125–9130.

Mountoufaris G, Canzio D, Nwakeze CL, Chen WV, Maniatis T. 2018. Writing, Reading, and Translating the Clustered Protocadherin Cell Surface Recognition Code for Neural Circuit Assembly. Annu Rev Cell Dev Biol 34:471–493.

Nicholson DA, Trana R, Katz Y, Kath WL, Spruston N, Geinisman Y. 2006. Distance-dependent differences in synapse number and AMPA receptor expression in hippocampal CA1 pyramidal neurons. Neuron 50:431–442.

Phillips GR, LaMassa N, Nie YM. 2017. Clustered protocadherin trafficking. Semin Cell Dev Biol 69:131–139.

Phillips GR, Tanaka H, Frank M, Elste A, Fidler L, Benson DL, Colman DR. 2003. Gamma-protocadherins are targeted to subsets of synapses and intracellular organelles in neurons. J Neurosci 23:5096–5104.

Prasad T, Weiner JA. 2011. Direct and Indirect Regulation of Spinal Cord Ia Afferent Terminal Formation by the γ-Protocadherins. Front Mol Neurosci 4:54.

Rubinstein R, Goodman KM, Maniatis T, Shapiro L, Honig B. 2017. Structural origins of clustered protocadherin-mediated neuronal barcoding. Semin Cell Dev Biol 69:140–150.

Schreiner D, Weiner JA. 2010. Combinatorial homophilic interaction between gamma-protocadherin multimers greatly expands the molecular diversity of cell adhesion. Proc Natl Acad Sci USA 107:14893–14898.

Wang X, Weiner JA, Levi S, Craig AM, Bradley A, Sanes JR. 2002. Gamma protocadherins are required for survival of spinal interneurons. Neuron 36:843–854.

Weiner JA, Wang X, Tapia JC, Sanes JR. 2005. Gamma protocadherins are required for synaptic development in the spinal cord. Proc Natl Acad Sci USA 102:8–14.

Wu Q, Maniatis T. 1999. A striking organization of a large family of human neural cadherin-like cell adhesion genes. Cell 97:779–790.

Zipursky SL, Sanes JR. 2010. Chemoaffinity revisited: dscams, protocadherins, and neural circuit assembly. Cell 143:343–353.

Figure 1

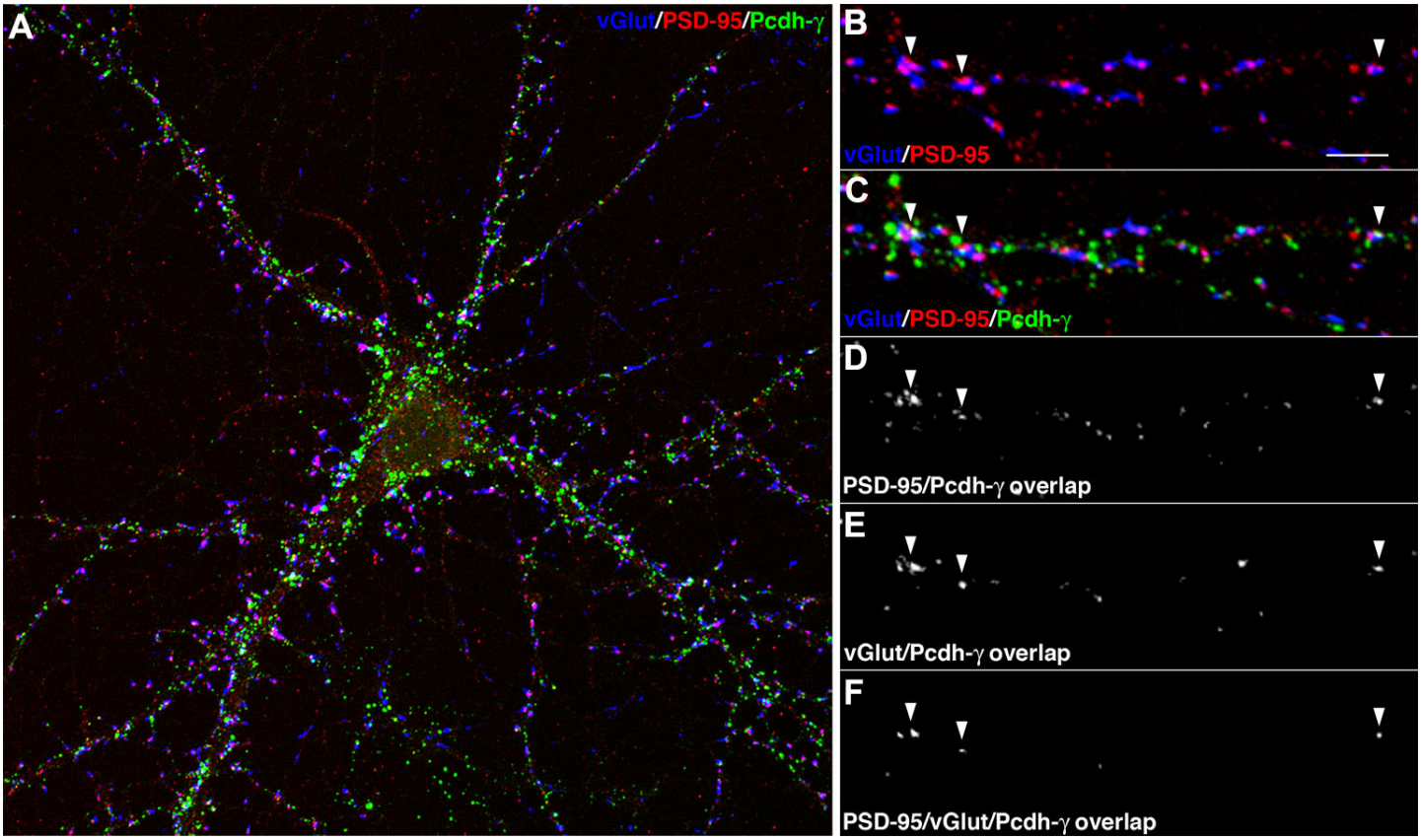
A
vGlut/PSD-95/Pcdh-γ
B
vGlut/PSD-95
C
vGlut/PSD-95/Pcdh-γ
D
PSD-95/Pcdh-γ overlap
E
vGlut/Pcdh-γ overlap
F
PSD-95/vGlut/Pcdh-γ overlap

Figure 2

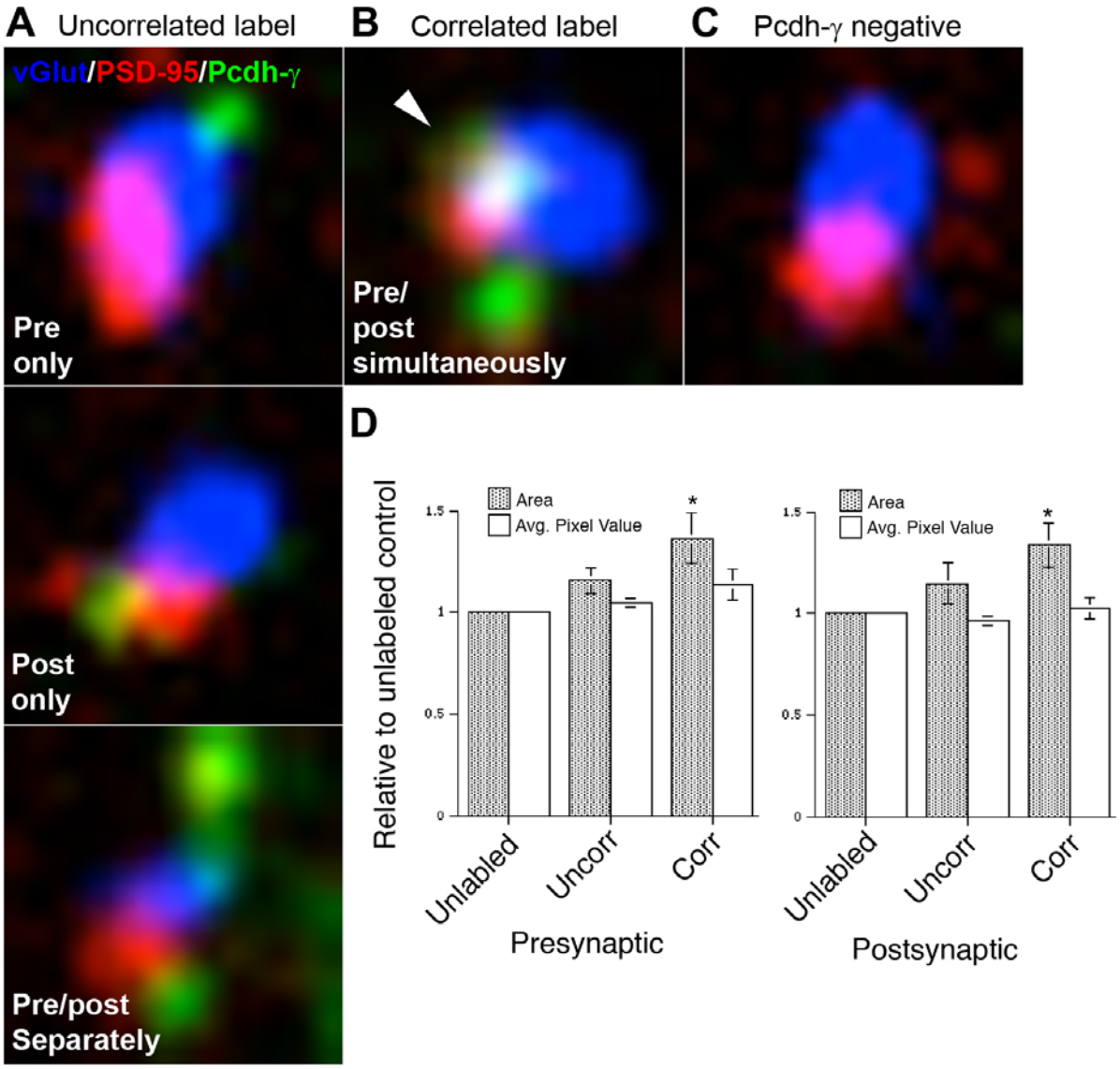
A Uncorrelated label
B Correlated label
C Pcdh-γ negative
vGlut/PSD-95/Pcdh-γ
Pre only
Pre/ post simultaneously
Post only
Pre/post Separately
D
Relative to unlabeled control
Area
Avg. Pixel Value
1.5
1
0.5
0
*
Unlabled
Uncorr
Corr
Presynaptic
Postsynaptic

Figure 3

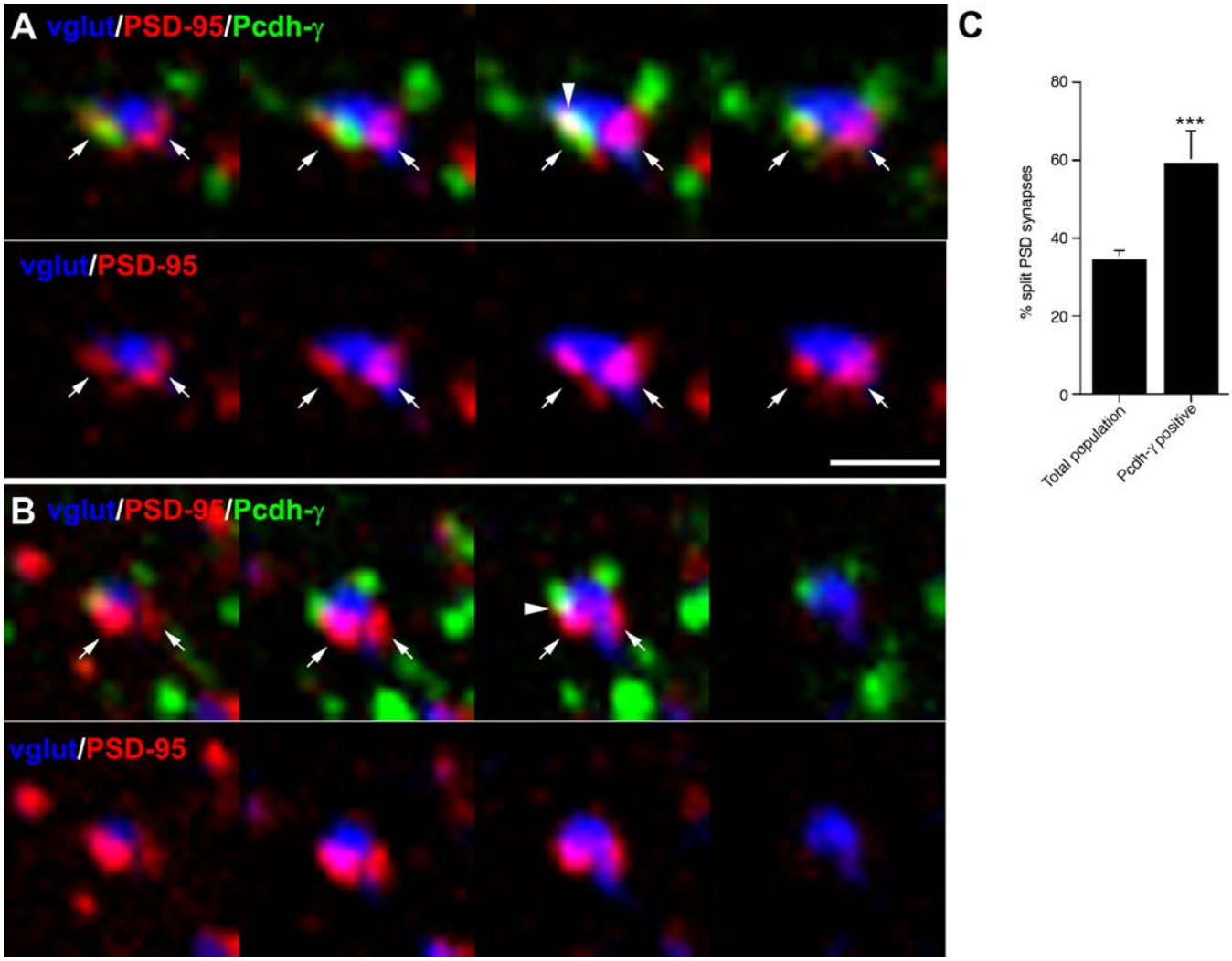
A vglut/PSD-95/Pcdh-γ
vglut/PSD-95
B vglut/PSD-95/Pcdh-γ
vglut/PSD-95
C
% split PSD synapses
80
60
40
20
0
***
Total population
Pcdh-γ positive

Figure 4

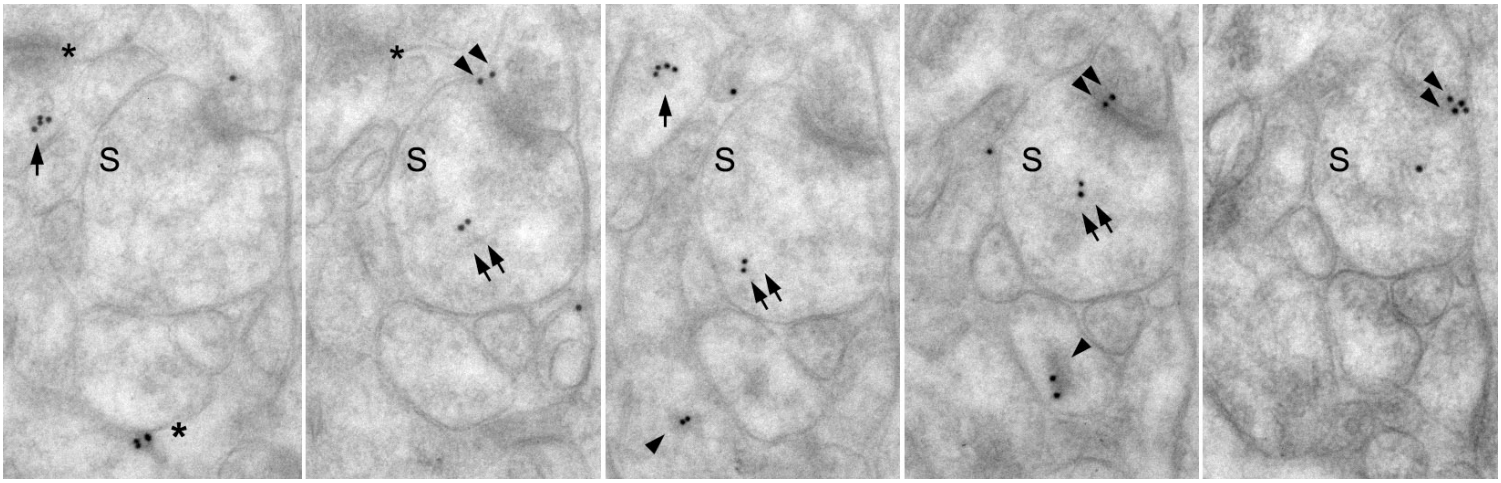

Figure 5

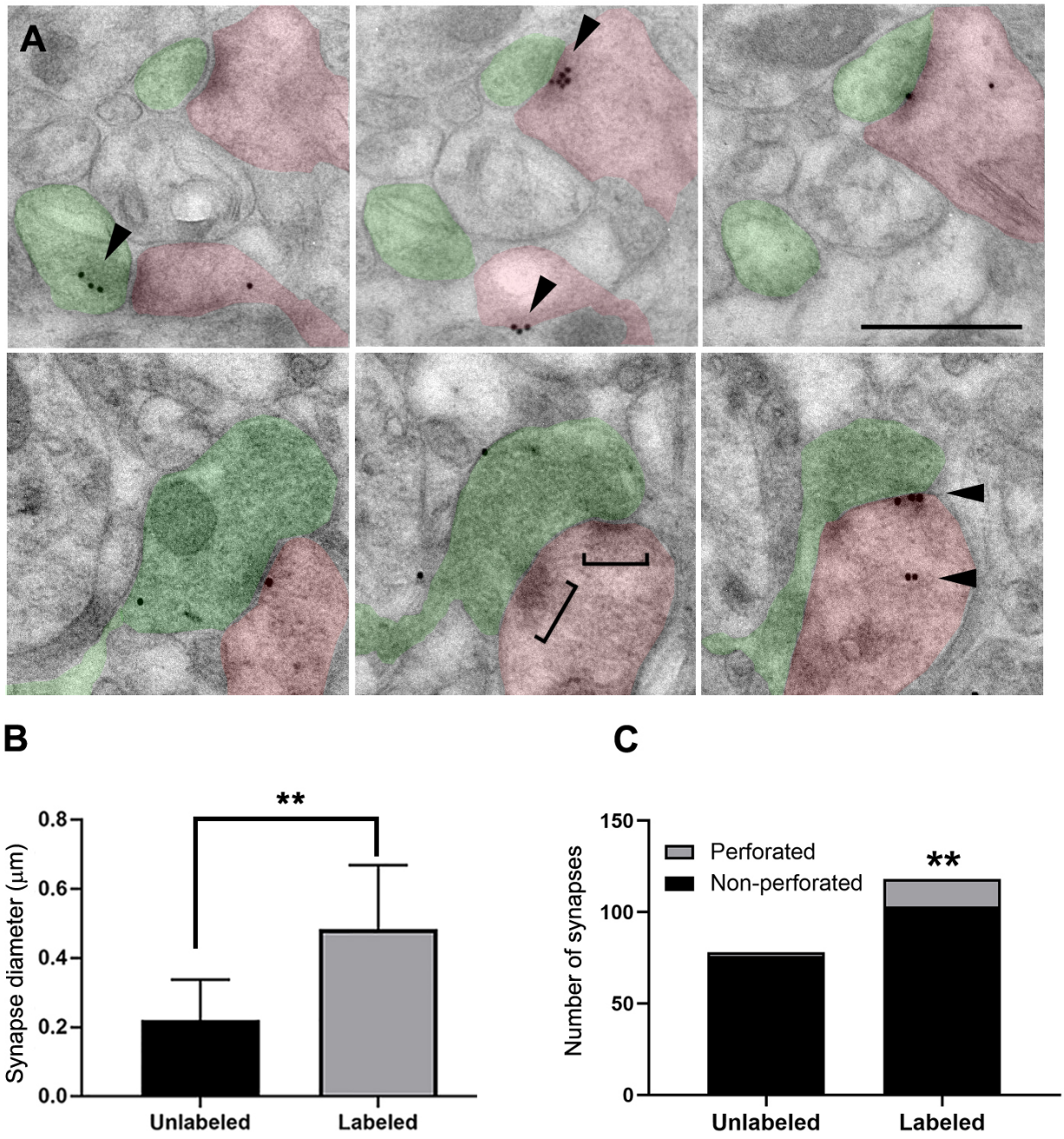
A
B
C
**
Synapse diameter (µm)
0.8
0.6
0.4
0.2
0.0
Unlabeled
Labeled
Perforated
Non-perforated
Number of synapses
150
100
50
0

Figure 6

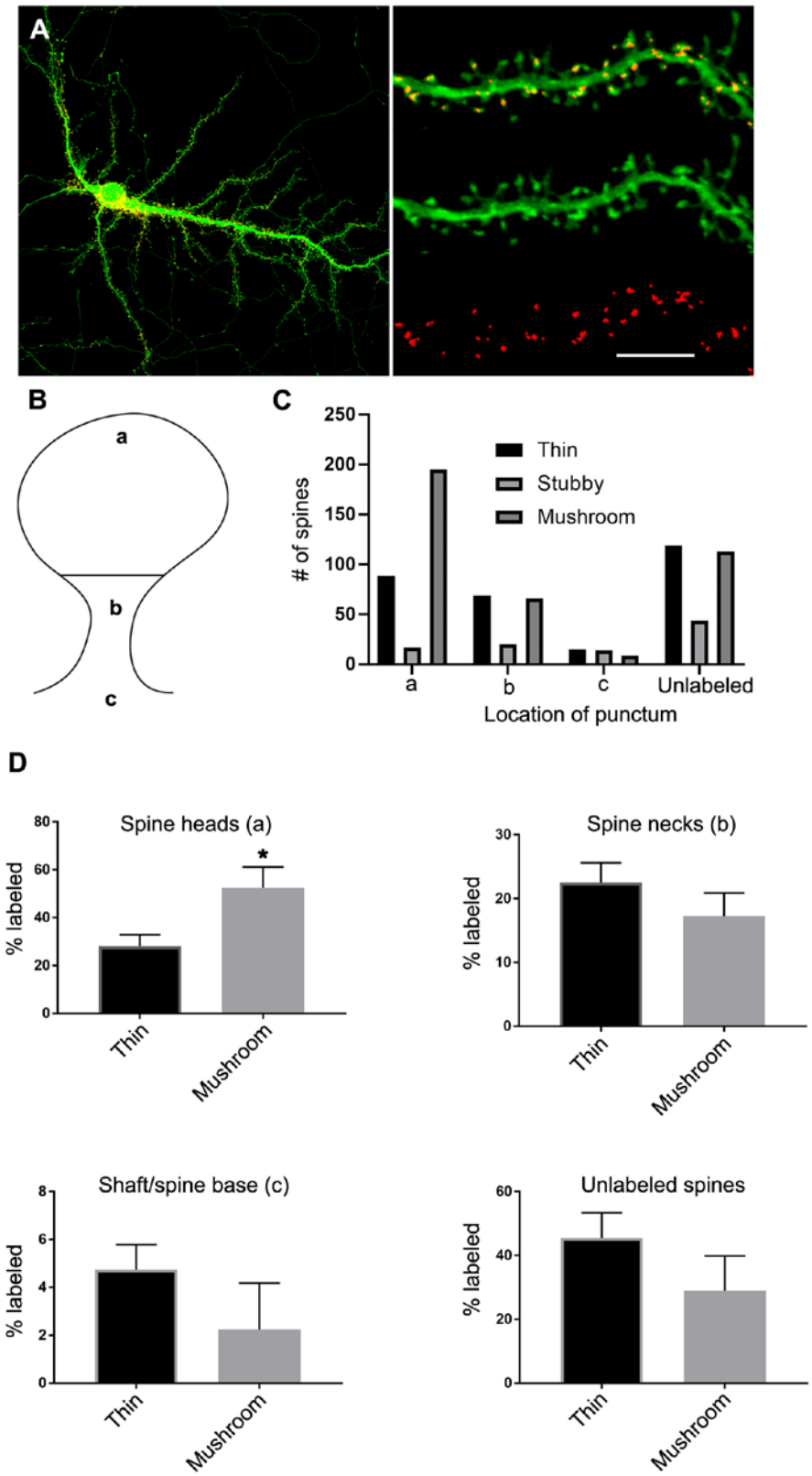
A
B
a
b
c
C
250
200
150
100
50
0
# of spines
Thin
Stubby
Mushroom
a
b
c
Unlabeled
Location of punctum
D
Spine heads (a)
80
60
40
20
0
% labeled
*
Thin
Mushroom
Spine necks (b)
30
20
10
0
% labeled
Thin
Mushroom
Shaft/spine base (c)
8
6
4
2
0
% labeled
Thin
Mushroom
Unlabeled spines
60
40
20
0
% labeled
Thin
Mushroom